

Article

A Novel Longwall Mining Layout Approach for Extraction of Deep Coal Deposits

Pengfei Wang ^{1,2,*}, Jingli Zhao ^{1,3}, Yoginder P. Chugh ^{2,4} and Zhiqiang Wang ¹

¹ College of Resource and Safety Engineering, China University of Mining and Technology (Beijing), Beijing 100083, China; zjl62331941@sina.com (J.Z.); wzhiqianglhm@126.com (Z.W.)

² Department of Mining and Mineral Resources, Southern Illinois University, Carbondale, IL 62901, USA; siu681@siu.edu

³ Russian Academy of Natural Sciences, Moscow 119991, Russia

⁴ Fellow, National Academy of Inventors, Tampa, FL 33612-9445, USA

* Correspondence: shengshikuangdaren@163.com or tbp140101030@student.cumtb.edu.cn

Academic Editor: Abbas Taheri

Received: 19 March 2017; Accepted: 12 April 2017; Published: 18 April 2017

Abstract: As more easily mined deposits are depleted, the reserves are becoming more limited and less favorable. Deposits of coal or trona that are being longwall mined are deep and are getting deeper. Coal bursts and bumps frequently occur within development entries in longwall mining of deep mines due to high stresses. This paper presents a novel patented longwall mining layout “Longwall Mining with Split-level Gate roads (LMSG)” that has the potential to mitigate several problems related to deep mining (Patent No. ZL98100544.6). LMSG locates gate roads on either end of a longwall panel at different vertical heights within a coal seam or in a geologically split seam, so that the two adjacent panels can be partially offset horizontally. It is novel in that it incorporates unit operations of different mining methods into the system. By employing multiple slice longwall mining method locally at the face ends, and adjacent panels overlapping end to end, pillar-less longwall mining can be achieved to mine deep deposits. A conventional rectangular gate road pillar is therefore transformed into a small triangular pillar and the gate road of the subsequent panel can be located along or under the gob of the previously mined panel where the stresses are lower. Several mines in China and Russia are currently using the technology with reduced incidence of ground control problems. Through theoretical analysis, and physical and numerical modeling approaches, it is demonstrated that LMSG significantly improves stress environment for development entries, with associated reduction in coal bursts and ground control problems.

Keywords: longwall layout; development entries; split-level; stress environment; ground control

1. Introduction

Longwall mining is a highly productive underground mining system. Relatively weak deposits such as coal and trona are using this system all over the world [1]. However, with time shallow reserves under adverse geologic conditions must be exploited to meet societal needs. Many coal mines in east China are mining at depths of more than 1000 m and their depths are increasing at a rapid rate. These mines are subjected to very high ground pressure that leads to ground control problems [2].

The stability of development entries or gate roads in longwall mining is essential to the safety and productivity of mining operations. A failure or collapse in gate roads can lead to accidents and/or interruption of mining operations with significant economic loss [3]. Gate roads and gate road pillars between longwall mining panels are subjected to a complex dynamic loading during their service life [4]. The use of conventional roof supports such as roof bolting and wire mesh may not be enough

for ground control [5]. Supplementary supports such as injection grouting, steel sets, and variations of pipe umbrella systems must be used to provide additional reinforcement that can incur high cost.

2. Stress Distribution Analysis for Longwall Panels

Due to the extraction of a longwall panel, uniformly distributed pre-mining stress is redistributed that results in abutment load ahead of the longwall face, side abutment load on the two sides of the panel and the rear abutment loading located in the compacted gob area [6,7]. Figure 1 shows side-view of stress redistribution after mining of one panel. It shows that abutment pressure along the positive x -coordinate axis increases exponentially with the distance from the origin and reaches peak abutment pressure at a certain distance x_0 that ranges from 3 to 20 m, and it lies typically between 5–12 m [6]. The peak pressure can reach up to five times the pre-mining vertical stress. The stress then decreases exponentially with the distance from the ribs. The stress on the solid coal on the right can be divided into four zones: I-De-stressed yield zone; II-Over-stressed plastic zone; III-Over-stressed elastic zone; and IV-Pre-mining vertical stress zone.

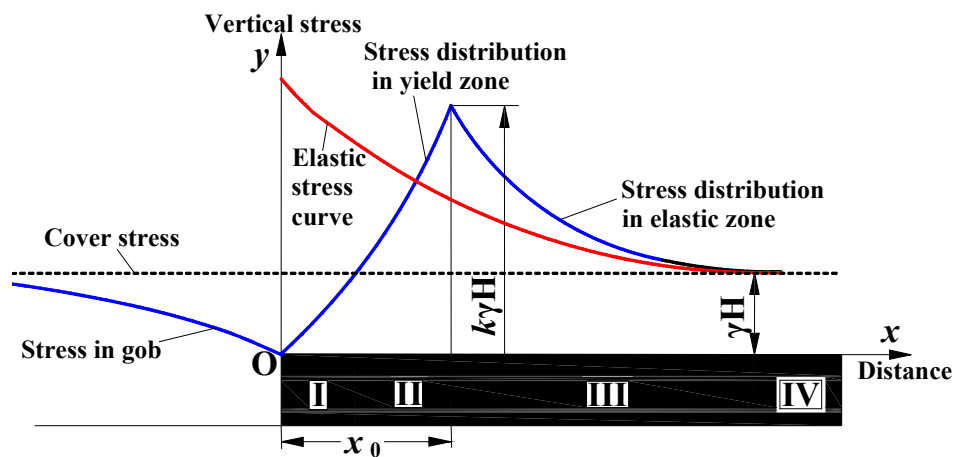


Figure 1. Side view of stress redistribution due to the extraction of a longwall panel (after [7]); k is stress concentration factor, H is cover depth, and γ is unit weight of overburden.

In typical longwall mining practice, gate roads and gate road pillars are placed along the floor (see Figure 2) and the gate road pillars are located in high pressure side abutment zones II or III (Figure 1) that can result in roof falls, coal bursts, and support problems. Large size gate road pillars are left between two panels so that the gate road of the new panel is located in zone IV or zone III (Figure 1) to avoid the influence of abutment pressures from adjacent mine workings. For example, Daizhuang coal mine at 600 m mining depth, the gate road pillars width is 70 m [8]; Yuhua coal mine with mining depth of over 450 m the gate road pillars width varies 60–100 m [9]. For a longwall panel with a long face advance, every small reduction in pillar width can improve economics in high production longwalls [10]. In addition to resource loss, gate road pillars also have higher probability of rock bursts [11]. Therefore, it would be beneficial if improved mining techniques can be developed that will improve stress environment for development entries and ensure high productivity and safety. This paper presents one such novel strategy with description of scientific foundations, mine design, physical and numerical modeling studies and field experience.

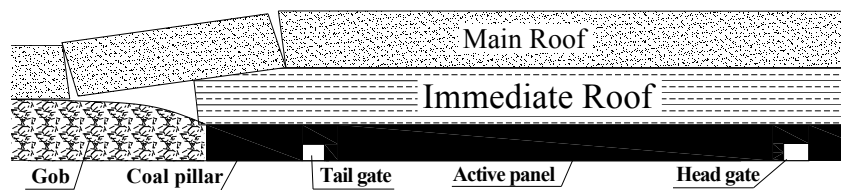


Figure 2. A typical conventional longwall panel layout [6].

3. Longwall Mining with Split-Level Gate Roads (LMSG): Overview

Figure 1 suggests that gate roads should be located in zones I or IV or within the gob area to be in relatively low stress environment than in zone II and III. Putting a gate road in zone IV will result in a large gate road pillars width while putting them in zone I will make them difficult to maintain due to complex loading during its life [12]. It is also difficult to drive a roadway through the gob although there have been a few cases [6]. Thus, in current longwall practice, there are limited areas for gate roads location.

Dr. Jingli Zhao at China University of Mining and Technology (Beijing) conceived the “Longwall Mining with Split-level Gate roads” (LMSG) or “Split-level Longwall Mining” (SLM) [13] that has been analyzed from ground control point of view since its conception [14–23]. LMSG locates gate roads on either end of the panel at different elevations. One gate road is driven along the floor while the other gate road is driven along the roof. Therefore, the longwall face has a gradually elevating section on one end of the panel. For the adjacent panel, the development entry may be located at the floor level either directly below the development entry of the previous panel or may be offset horizontally with respect to it.

Figures 3 and 4 show a typical two-entry LMSG top coal caving mining layout in relatively flat coal seams. Figure 3 shows the gate roads on both sides of the active panel (Panel 1) to be split level. The tail gate 1 is driven right above the floor level while the head gate 2 is driven right below the roof with gradually elevating Section 5 on one end of the panel. This part is elevated incrementally by adjusting the inclination of each section of the armored face conveyor (AFC), shields and other production machines. The length and inclination of each AFC section are typically 1.5 m and 3° and Figure 4 shows that the inclination is small. Figure 3 shows that the tail gate 3 of the successive panel (Panel 2) is driven along the floor similar to tail gate 1. A small pillar with a triangular x -section is left unmined along the edge of the mined-out area after mining of Panel 1.



Figure 3. Typical LMSG (Longwall Mining with Split-level Gate roads) top coal caving mining layout in relatively flat coal seams (Figure prepared courtesy of Zhao [13]). 1—Tail gate of the active panel (Panel 1); 2—Head gate of the active panel (Panel 1); 3—Tail gate of the successive panel (Panel 2); 4—Head gate of the previous panel (Panel 1); 5—Triangular x -section coal pillar loss.



Figure 4. 3D view of shield layout for one LMSG panel.

Mining operations in LMSG termed “Triple Sections Mining Technology” (TSMT) [24] are shown in Figure 5. The working of section “a” is performed under an artificial roof or pseudo-roof or regenerated roof with steel mesh underneath and is constructed when mining the upper level of the same section of the previous panel. The load-deformation characteristics of the artificial roof depend upon the volume of the caved rocks mass under the caving line, their frictional and cementation properties and the resulting bridging structures formed by roof strata.

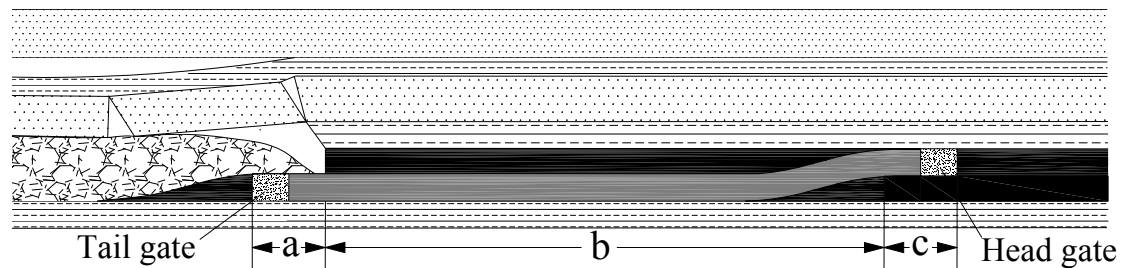


Figure 5. Triple sections mining technique (TSMT) for LMSG top coal caving (Figure prepared courtesy of Zhao [24]).

Therefore, the tail gate development for the new panel within section “a” is done under the steel wire meshed artificial roof and with two sides of solid coal (one side is the rib of the triangular x-section coal pillar, and the other side rib of the solid coal bed). The tail gate is supported by steel sets with wire mesh on the top preventing the caved rock fragments from falling. Therefore, the support system thus has to carry only the load of the caved rock mass [22]. Mining operations in section “b” are similar to conventional longwall top coal caving (CLTCC) while the working of section “c” is similar to multi-slice longwall mining technology. The shield support has a wire mesh laying device on the top to form an artificial roof for the next section “a” of the next new panel. Since the roof rock in the head gate is more competent than the soft coal, roof support requirements are not very large.

The distinct difference between LMSG and standard methods is that there are three operations in LMSG: meshing operation used in multi slice longwall mining method in section “c”, longwall top coal caving operation in section “b” (coal cutting and top coal caving) and coal cutting operation in section “a” under the steel wire meshed artificial roof. However, for a multi slice longwall mining method, the operation throughout the face is the same, that is, coal cutting and steel wire meshing (to form steel wire meshed artificial roof for the lower slice(s)).

4. Case Study Utilizing LMSG

Huafeng coal mine 1410 longwall panel in Shandong province uses LMSG because of over 1000 m mining depth. The coal seam is about 6.2 m thick with average inclination of 32° that can result in sliding of the production equipment on the face. The mine experienced over 100 incidences of coal bursts that led to deaths of at least five and injured more than 43 workers. Over 75% of the bursts occurring in gate roads. All bursts in tail gates were only one pillar width away from the gob of the previously mined-out panel. It is well established that the key to preventing the bursts in gate roads is to minimize overstressing of gate road pillars [6]. Even though the size of the gate road pillars was incrementally reduced at this mine from 20 m to 10 m, 7 m, and 5 m, bursts continued to occur. Therefore, the LMSG method was adopted with the panel layout shown in Figure 6.

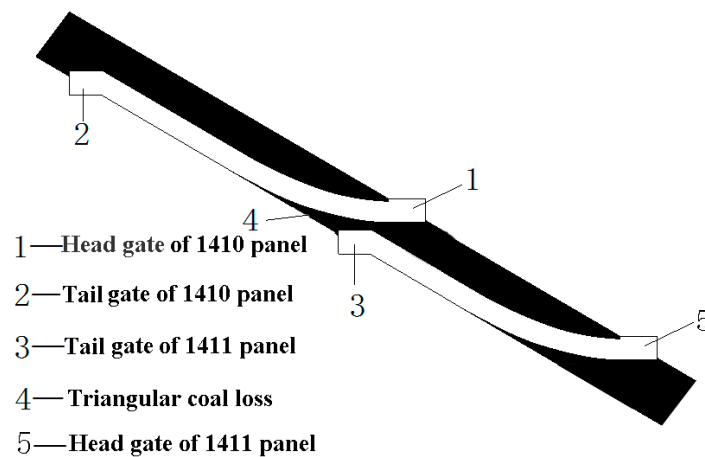


Figure 6. Panel layout for Huafeng Mine 1410 and 1411 longwall panels.

Advantages of LMSG layouts: Since the tail gate of the active panel is located in a de-stressed zone, roof support requirements are small. Since the mining height of the previously mined panel close to the head gate of the panel becomes smaller with distance, the stress concentrations within solid coal ahead of the active longwall face close to the head gate of the previous panel are smaller compared with CLTCC due to the larger mining height [6]. In effect, the stress concentration is within the solid coal ahead of the working face of the active panel. Furthermore, shield supports on a longwall face are designed to sustain high loads over a small area, but it is difficult to deal with the highly stressed environment in gate roads that result in ground control problems. The extensive field experience with LMSG in China [11,14–23] corroborates the above statement.

According to literature [6,21], the width of the gate road pillars in China is calculated by:

$$B = x_0 + 2m + x_1, \tag{1}$$

where B = width of gate road pillars; x_0 = width of plastic or yielded zone adjacent to the gob; m = mining height; and x_1 = the width of plastic or yielded zone adjacent to the next new roadway:

$$x_0 = \frac{m}{2\xi f} \ln \frac{k\gamma H + C \cot \varphi}{\xi(p_1 + C \cot \varphi)}, \tag{2}$$

where f = coefficient of friction; φ = angle of internal friction; C = cohesion; γ = unit weight; H = cover depth; k = stress concentration factor; p_1 = force of steel sets acting on the rib; and $\xi = \frac{1+\sin \varphi}{1-\sin \varphi}$.

Zhao [21] reported that the distance x_0 in Figure 1 is much smaller in LMSG than in CLTCC since the mining height “ m ” is reduced. Figure 7 shows that since the tail gate is now driven in section V, the vertical stress is less than the pre-mining vertical stress. Since the lost solid triangular x -section pillar is located on the negative half of the x -axis (“negative coal pillar”), the coal loss is significantly reduced since the original “T” shape coal loss is reduced to a triangular x -section.

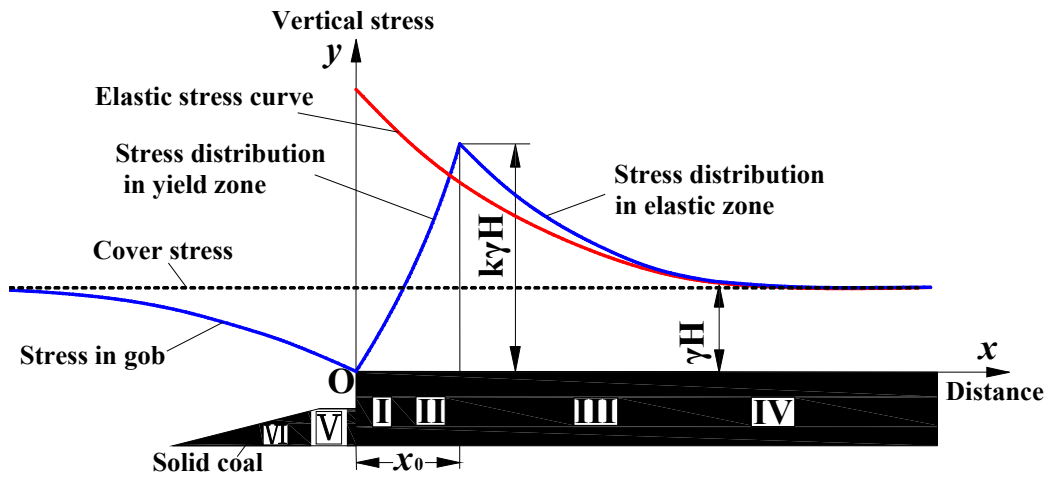


Figure 7. Stress redistribution after the excavation of a LMSG panel on one side; k is stress concentration factor, H is cover depth, and γ is unit weight of overburden.

LMSG can be applied in medium-thick, thick or ultra-thick coal seams. With the development of tunneling technology, gate roads in weak rocks can be driven at a relatively low cost. Therefore, LMSG can also be applied in low thickness coal seams with high extraction ratio and high productivity as shown in Figure 8. In such cases, the head gate can be driven within or partially within the immediate roof rock [23].

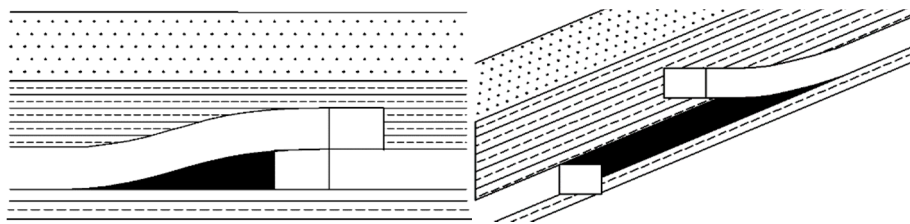


Figure 8. Head gate driven within immediate roof or main roof rock bed.

LMSG can also be used to minimize the surface deformations and damage to surface structures. The remnant gate road pillars in CLTCC can result in wavy surface deformations above multiple isolated panels with gate road pillars between them. With LMSG, the conventional large gate road pillars are absent, and only small triangular x -section coal pillars are left that (Figure 9) result in relatively uniform subsidence shown in Figure 10. The LMSG can also provide good results in protecting surface structures in deep mines where CLTCC with gate road pillars between two panels may not provide critical mining width. With LMSG, isolated subsidence troughs over individual panels will ultimately join together to form a large flat-bottomed trough to reduce surface deformation strains.



Figure 9. A comparison of coal loss in conventional and LMSG mining systems.

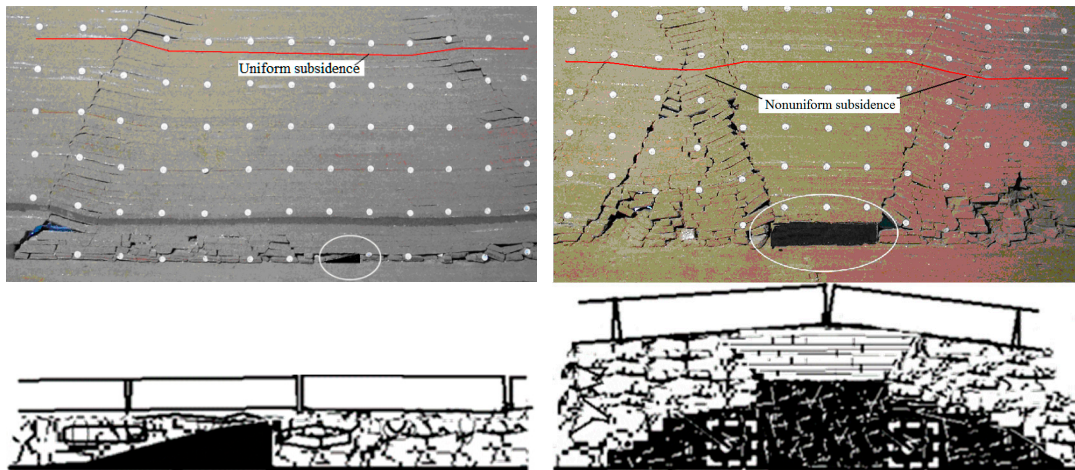


Figure 10. Characteristics of surface subsidence with LMSG and its comparison with CLTCC (conventional longwall top coal caving) (Figure prepared courtesy of Fan [22]).

In inclined and steeply-inclined seams, LMSG can solve operational problems such as sliding of mining equipment downhill, and disconnection of armored face conveyor (AFC) to the stage loader because the lower end of the working face becomes flat. Hebi [16], Tangshan [15,18], Gongwusu [19], Jingyuan [20], etc. have adopted LMSG to solve these problems as shown in Figures 11 and 12. The application of LMSG in Dongxia Mine uses LMSG that provides control on the overall stability of the supports on a steeply inclined working face (up to 52°). The lateral force between the supports decreases in the flat section of the mining face and reduces to a minimum in the level section. This increases the support efficiency as shown in Figure 13. The LMSG can have many options for designing mining layouts (Figure 14) such as: (a) vertical overlapped entries; (b) external overlapped entries; (c) external spaced overlapped entries; (d) staggered configuration with coal sheet between two panels; (e) spaced configuration in inclined seams; (f) LMSG configuration in flat thin coal seam; and (g) LMSG configuration in inclined thin coal seam.

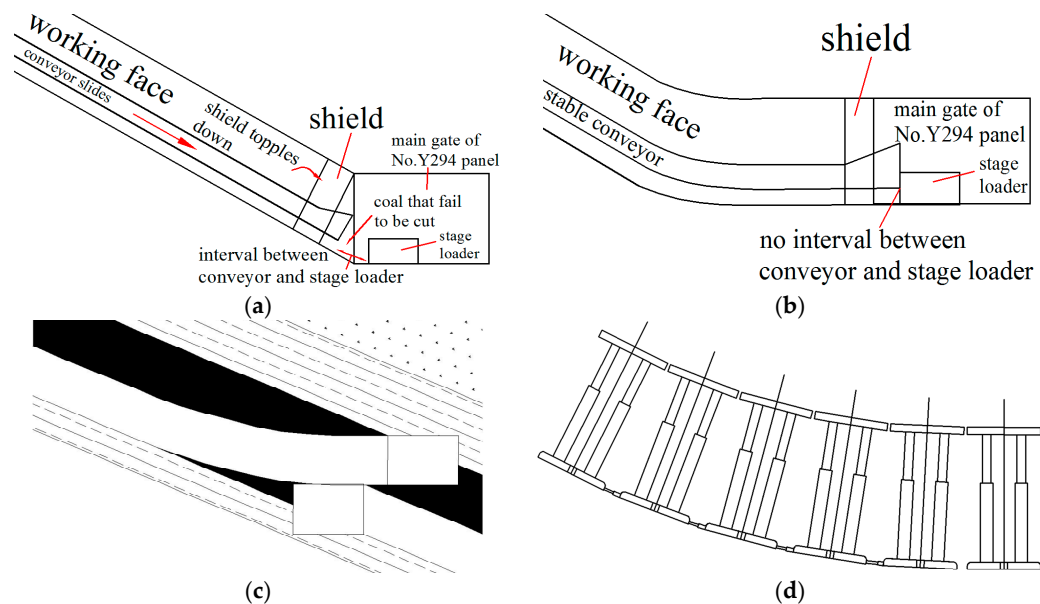


Figure 11. Application of LMSG in Tangshan coal mine, China [15]. (a) Conventional layout; (b) LMSG layout; (c) panel continuance; (d) shield transition.

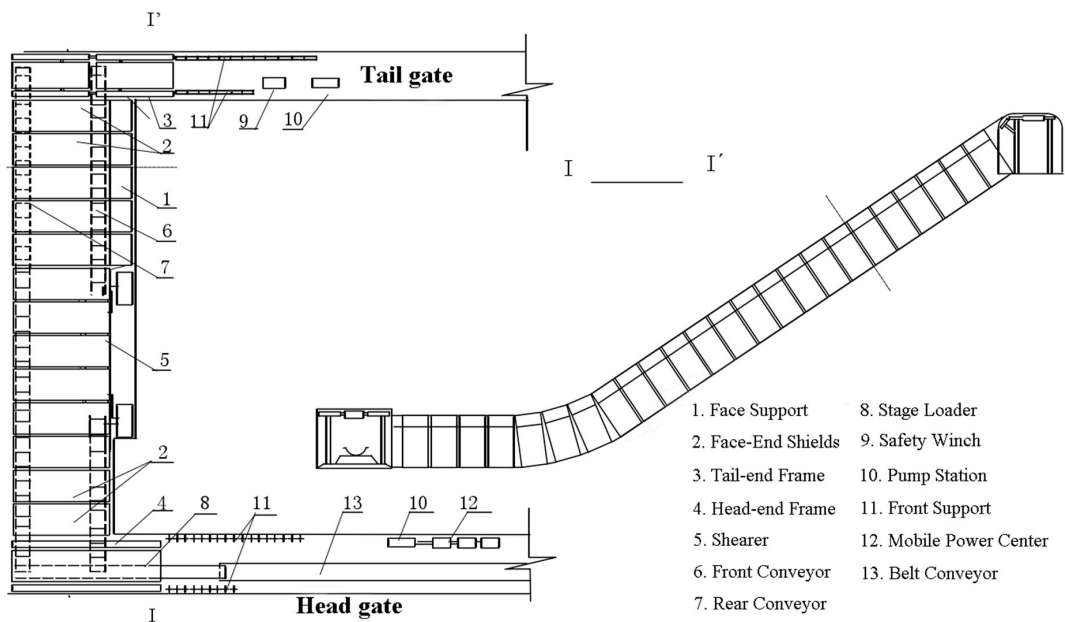


Figure 12. Application of LMSG in Jingyuan coal mine, China.

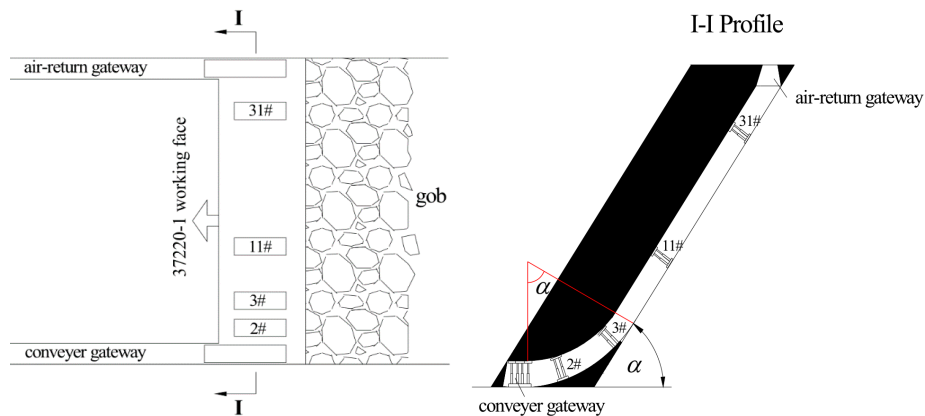


Figure 13. LMSG in Dongxia Coal Mine, Huating coal field, Gansu province, China ($\alpha = 52^\circ$).

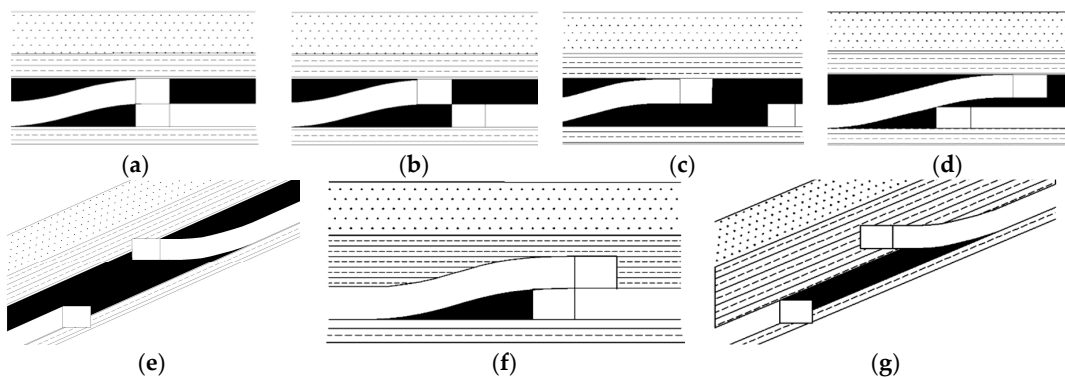


Figure 14. Commonly used LMSG patterns. (a) Vertical overlapped entries; (b) external overlapped entries; (c) external spaced overlapped entries; (d) staggered configuration with coal sheet between two panels; (e) spaced configuration in inclined seams; (f) LMSG configuration in flat thin coal seam; (g) LMSG configuration in inclined thin coal seam.

5. Ground Control Studies of LMSG Using Physical Models

Physical modeling has been extensively used in China to study strata behavior [25] and it has also been used to analyze the LMSG. At one of the case study mines, two 50 mm diameter core holes were drilled from underground workings to develop engineering properties. The No. 1 core hole was drilled in the head gate of 1411 panel, while the No. 2 core hole was drilled in the tail gate. The developed engineering properties are given in Table 1 and were used to develop equivalent model materials properties for physical models. Similitude equations for equivalent model materials strength, density and geometry are given below [26]:

$$\frac{C_\sigma}{C_\rho \times C_L} = 1, \quad (3)$$

where C_L is the geometric scaling constant, C_σ is a constant of strength similarity and C_ρ is a constant of density similarity for the prototype (full scale case) and the model. The constants C_L , C_σ and C_ρ were calculated as follows:

$$C_L = \frac{L_p}{L_m}, C_\sigma = \frac{\sigma_p}{\sigma_m}, C_\rho = \frac{\rho_p}{\rho_m}, \quad (4)$$

where subscript p represents the prototype; m represents the model; L is the length; σ is the strength; and ρ is the bulk density.

For physical model development, geometric scaling factor of C_L of 1:200, and density factor of $C_\rho = 1:1.6$ was used. The model materials consist of aggregate (fine sand) and cement materials (lime and Plaster of Paris). The proportion of different constituents in the model materials are given in Table 2. Strain gages were embedded into model materials appropriately to measure strains.

Two large-scale physical models, representing plane-stress simulation, were developed. The model dimensions were 162 cm long, 130 cm high and 16 cm thick (Figure 15). Simulated mining depth and panel widths were 1000 and 100 m. A strain gauge indicator was used to collect strain data, which was converted to stress values using stress–strain relationships. Stress concentration in abutment zones was measured using stress sensors and a digital data acquisition system. Development entries and face were excavated in 2 m slices. The excavation of the first and the second panel are shown in Figures 16 and 17.

Table 1. Engineering properties of rock cores from Boreholes 1 and 2.

Lithology	Height (m)	Density (kg/m ³)	Modulus of Elasticity (MPa)	Poisson's Ratio	Internal Friction Angle (°)	Tensile Strength (MPa)	Cohesion (MPa)	UCS (Uniaxial Compressive Strength) (MPa)
Fine grained sandstone	56.0	2500	22,000	0.22	40	6.0	6.2	73.6
Medium grained sandstone	12.0	2500	23,000	0.23	42	6.2	6.4	76.0
Siltstone	4.0	2570	35,000	0.22	38	5.8	5.3	39.0
Medium grained sandstone	6.0	2500	23,000	0.23	37	6.0	6.4	66.0
Fine grained sandstone	10.0	2500	22,000	0.22	40	6.0	6.2	73.6
Coal seam	6.2	1450	3100	0.25	23	1.2	0.8	15.0
Siltstone	2.1	2570	35,000	0.22	38	5.8	5.3	39.0
Ultra-fine grained sandstone	2.7	2600	37,000	0.22	36	5.3	5.8	57.0

Table 2. Material parameters and proportion of different constituents in physical model materials.

Rock Types	UCS (MPa)	Unit Weight (kg/m ³)	Proportion Number	Materials	Aggregate: Materials	Lime:Plaster (Lime:Soil)
Medium grained sandstone	0.058	1667	6:5:5	fine sand:lime:plaster	6:1	7:5
Fine grained sandstone	0.056	1667	8:6:4	fine sand:lime:plaster	7:1	6:4
Ultra-fine grained sandstone	0.044	1733	7:6:3	fine sand:lime:plaster	7:1	5:4
Siltstone	0.03	1713	6:5:5	fine sand:lime:plaster	6:1	5:5
Coal seam	0.011	967	10:1:0	fine sand:lime:soil	10:1	7:2

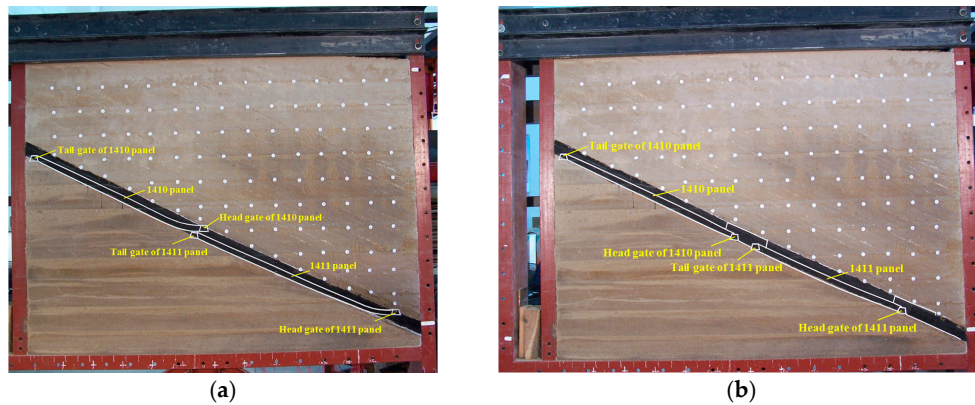


Figure 15. Physical models. (a) LMSG; (b) CLTCC.

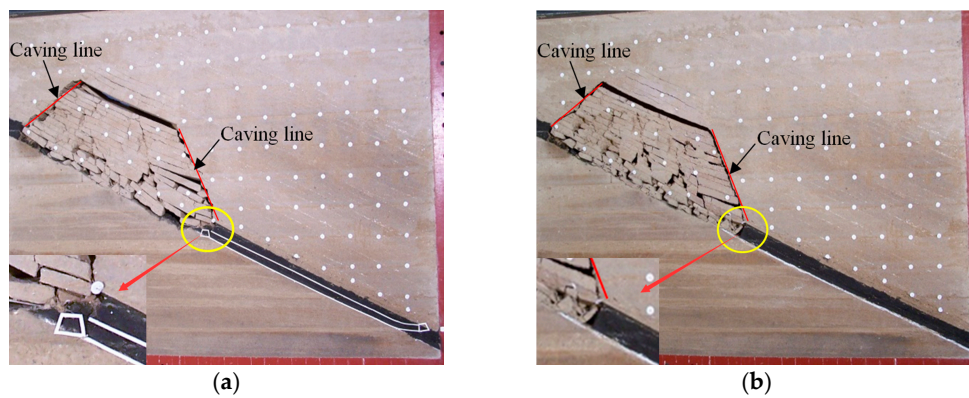


Figure 16. Excavation of 1410 panels in physical models. (a) LMSG; (b) CLTCC.

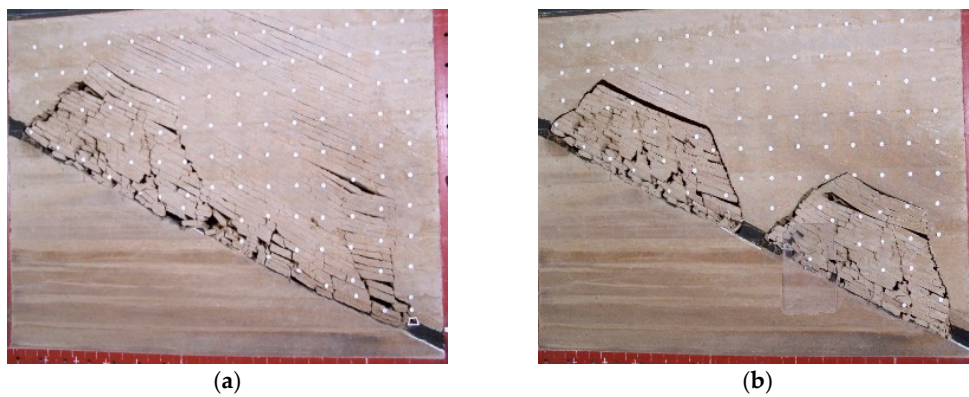


Figure 17. Excavation of 1411 panels in physical models. (a) LMSG; (b) CLTCC.

6. Modeling Results and Discussion

Figure 16a,b show that excavations of the first panels, i.e., 1410 panels employing LMSG and CLTCC are similar except the difference of geometries of the lower face ends. Figure 16a shows that the LMSG face end has a transition from incline to flat while Figure 16b shows that the CLTCC face end has an abrupt right angle. Figure 16a also shows that the tail gate of the adjacent panel is located right under the edge of the gob of the previous panel. Since the caved strata over this part typically bridges, a protective arch structure is developed over the tail gate. Stress distribution data are shown in Figures 18 and 19. The stress around this tail gate is much lower than the pre-mining stress and therefore the likelihood of ground control problems is reduced. This concept is similar to the advice that the safest place in a room during earthquake is a corner where a bridge protective structure is likely to form. Figure 17a shows that since there is no pillar between two adjacent panels, the overlying strata across the two panels subside or deform as a unit after extraction of the two panels and the gobs of the two panels connect with each other with only a negligible triangular x -section coal pillars between them. Thus, it behaves as if it were a super-critical longwall panel. In the CLTCC, the gate road pillars between panels has non-uniform stress distribution with associated non-uniform strata movement with wavy or irregular surface subsidence deformations (Figure 10).

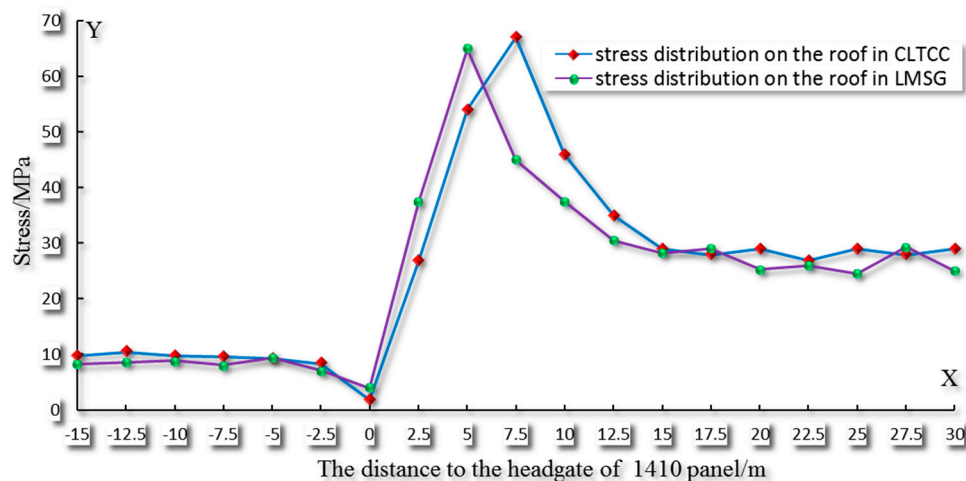


Figure 18. Stress distribution in the immediate roof after excavation of the 1410 panel (physical model).

It can be seen from Figure 18 that the pre-mining stress is about $1000 \text{ m} \times 0.025 \text{ MPa/m} = 25 \text{ MPa}$, while the maximum stress in the gob is only about 10 MPa. This is most likely due to the pressure of the caved strata below the relatively intact key stratum [6]. Most importantly, at the edge of the gob (between 0 to -5 m along the x -axis), the stress is significantly reduced even below the other parts of the gob. Therefore, the tail gate of the successive panel is in a destressed zone. This is the most destressed part in the entire panel layout system and therefore ground control problems should be reduced. Since there are no gate road pillars between the panels, the gobs of the two panels connect with each other, and the small remnant triangular coal pillar has little effect on stress distribution in the gob. Thus, the strata above the two panels deform down together as a unit, the key strata also moves downward and the intact key strata is higher. The caved zone is increased and the gob is more uniformly loaded with higher gob pressure shown in Figure 19. However, at the edge of the gob between 0 to about -5 m along the x -axis, the stress is independent of gob volume and therefore it is a perfect location for the gate road(s).

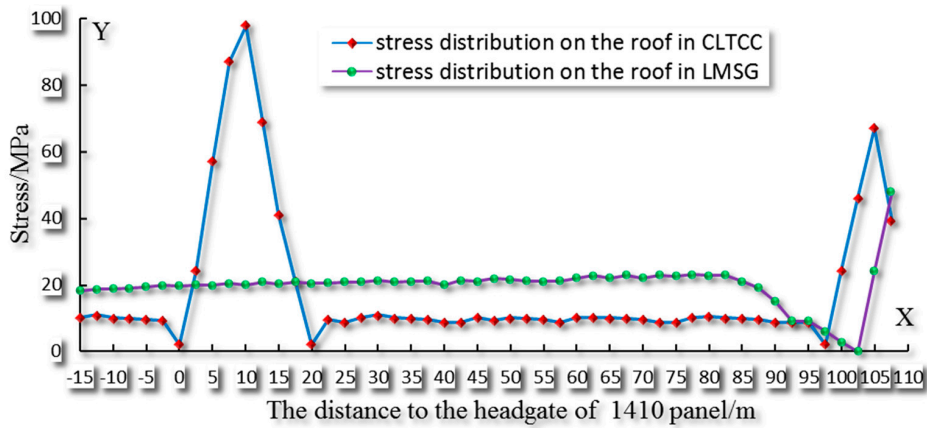


Figure 19. Stress distribution in the immediate roof after excavation of the 1411 panel (physical model).

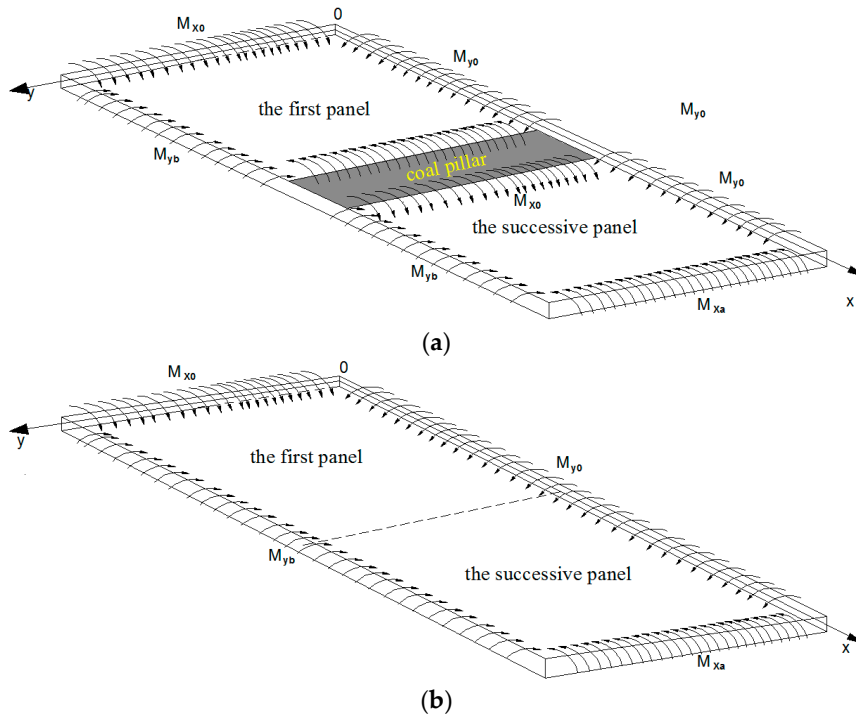


Figure 20. Key strata structural models for LMSG and CLTCC. (a) Key strata structural model for CLTCC; (b) key strata structural models for LMSG.

Based on the key stratum theory [6] and elastic theory of thin plates [27], the structural model was developed for Huaifeng mine as shown in Figure 20. In conventional longwall mining, gate road pillars between adjacent panels are left, adjacent panels are relatively independent of each other and strata above form two plates with four edges of each plate clamped rigidly at four edges. While in LMSG no pillar is left between two panels, two rectangular plates above them form a single plate with four edges rigidly clamped at four edges. The stability of the plate depends on length and width of the overhanging plate. The length “a” depends on panel length and the number of panels; and width “b” depends on the face advance distance. The plate deflection is given by [28]:

$$\omega = \frac{7q \cos \theta}{128(a^4 + 7a^2b^2 + b^4)D} (x^2 - a^2)^2 (y^2 - b^2)^2, \tag{5}$$

where ω is deflection function; q is uniform load acting on the plate; θ is inclination of the coal seam; a , b -length and width of the stable key strata, respectively; and D is flexural rigidity of the plate.

If the plate is treated as a combination of several strip beams, then the bending moment along x and y axes are given below:

$$M_x = D \frac{d^2\omega}{dx^2} = \frac{14q \cos\theta (y^2 - b^2)^2}{128(a^4 + b^4 + \frac{4}{7}a^2b^2)} (6x^2 - 2a^2), \quad (6)$$

$$M_y = D \frac{d^2\omega}{dy^2} = \frac{14q \cos\theta (x^2 - a^2)^2}{128(a^4 + b^4 + \frac{4}{7}a^2b^2)} (6y^2 - 2b^2). \quad (7)$$

When the thin plate fractures, deflections are equal, i.e., $M_x = M_y$. From Equations (6) and (7), only when $x = y$, $M_x = M_y$, which means it tends to break when the plate is rectangular. If we set $b = \lambda a$, then:

$$M_{\max} = \frac{7q \cos\theta \lambda^2 a^2}{16(1 + \frac{4}{7}\lambda^2 + \lambda^4)}. \quad (8)$$

As $\sigma_{\max} = \frac{M_{\max}}{W_{\max}} \leq [\sigma]$, i.e., $M_{\max} \leq W_{\max} \cdot [\sigma]$, and $W_z = \frac{b'h^2}{6}$ [29], where W is the elastic section modulus; and b' and h are the width and height of the section, respectively. Setting $b' = 1$ unit, then:

$$M_{\max} = \frac{7q\lambda^2 a^2}{16(1 + \frac{4}{7}\lambda^2 + \lambda^4)} \leq \frac{h^2}{6} [\sigma]. \quad (9)$$

This indicates that the key stratum will break when maximum normal stress exceeds its tensile strength. Stability conditions of the key strata above panels are obtained through the above equations. In CLTCC, key strata above panels are isolated and independent of each other but in LMSG, they are connected and deform as a single unit. Therefore, for the same size of the thin plates, intact key strata in LMSG will be higher than in CLTCC as discussed earlier (see Figure 21).

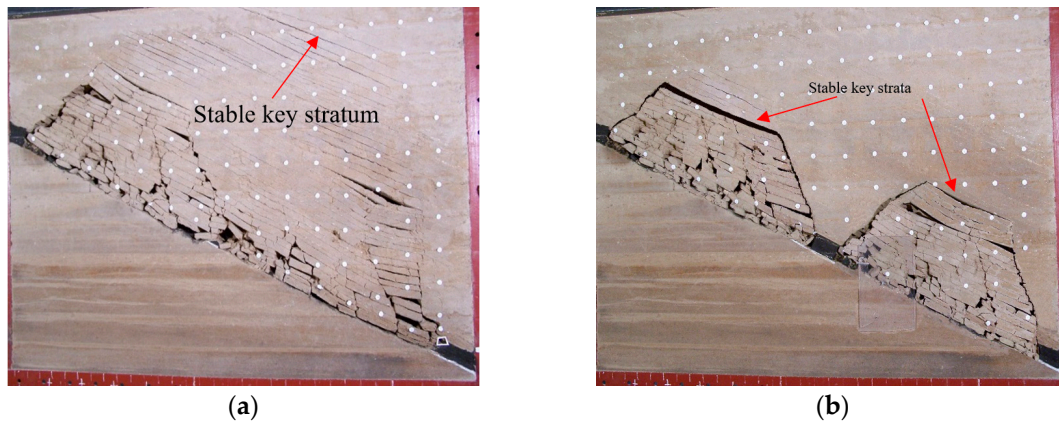


Figure 21. Key strata characteristics of the LMSG and CLTCC methods. (a) LMSG; (b) CLTCC.

7. Analysis of LMSG Mining Layouts Using Numerical Modeling

Rock and Soil 2D software or RS2 (Phase2 8.0) [30] finite element software was used. The constitutive models in the program include Mohr–Coulomb, Generalized Hoek–Brown (GHB) and Cam–Clay. Additional features include modeling of jointed rock with automatic generation of

discrete joint or fracture networks using statistical models. The widely used GHB failure criterion was adopted for all analytical studies [31,32] which is expressed as:

$$\sigma_1 = \sigma_3 + \sigma_{ci} \left(m_b \frac{\sigma_3}{\sigma_{ci}} + s \right)^a, \tag{10}$$

where σ_1 = major principal effective stress at failure; σ_3 = minor principal effective stress at failure; m_b = the value of the constant m for broken rock; m = constant depending on the characteristics of the rock mass; s = constant depending on the characteristics of the rock mass, ranging between 0~1; a = constant for broken rock; and σ_{ci} = uniaxial compressive strength (UCS) of intact rock material. Furthermore,

$$m_b = m_i \exp\left(\frac{GSI - 100}{28 - 14D}\right), \tag{11}$$

$$s = \exp\left(\frac{GSI - 100}{9 - 3D}\right), \tag{12}$$

$$a = \frac{1}{2} + \frac{1}{6} \left(e^{-GSI/15} - e^{-20/3} \right), \tag{13}$$

where GSI = geological strength index; and D = disturbance factor, which depends upon the degree of disturbance due to blast damage and/or stress relaxation varying from 0 for undisturbed in-situ rock mass to 1 for very disturbed rock masses. The rock mass engineering parameters were developed based on estimated GSI values and RocData software and were used to assess the effect of engineering properties on failure behavior [33]. The GHB parameters (σ_{ci} , m_i and a) were obtained from Figure 22. An elastic-plastic model was adopted for post-peak behavior. Pre-mining stress measurements in the mine showed maximum horizontal stress to be about 1.7 to 2.0 times the vertical stress. Rock mass engineering properties used for numerical modeling are given in Table 3.

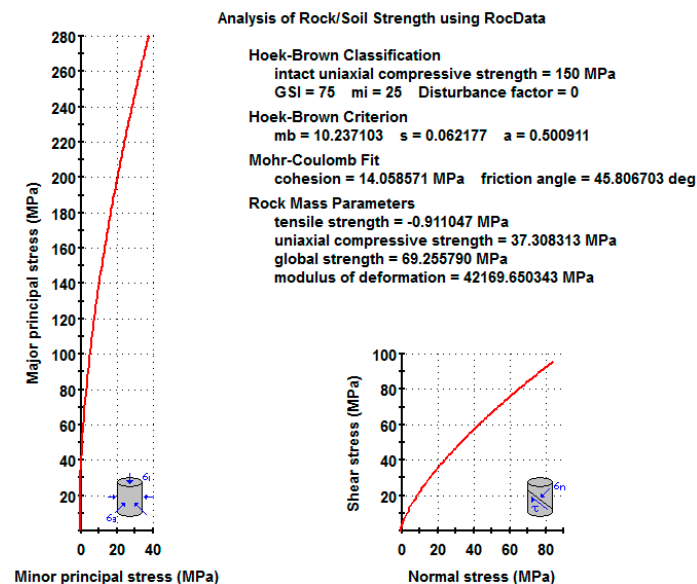


Figure 22. Estimation of rock mass strength parameters using RocData software.

Table 3. Rock mass engineering parameters used in numerical modeling.

Lithology	Thickness (m)	Young's Modulus/GPa	Poisson's Ratio λ	σ_{ci}/MPa	GSI (Geological Strength Index)	m_i	m_b	s	a	Dilation
Top	-	40	0.23	150	85	25	14.631	0.1889	0.5004	1.2
Fine grained sandstone	56	20	0.22	120	72	17	6.254	0.0446	0.5012	1.5
Medium grained sandstone	12	32	0.23	130	75	19	7.780	0.0622	0.5009	1.3
Siltstone	4.0	18	0.24	40	65	16	4.584	0.0205	0.5020	1.5
Medium grained sandstone	6	32	0.23	130	75	19	7.780	0.0622	0.5009	1.3
Fine grained sandstone	10	20	0.22	120	72	17	6.254	0.0446	0.5012	1.5
Coal seam	6.2	3.1	0.25	30	60	15	3.595	0.0117	0.5028	2.0
Siltstone	2.1	18	0.24	40	65	16	4.584	0.0205	0.5020	1.5
Ultra-fine grained sandstone	2.7	20	0.22	80	70	18	6.165	0.0357	0.5014	1.3
Fine grained sandstone	10	20	0.22	120	72	17	6.254	0.0446	0.5012	1.5
Medium grained sandstone	12	32	0.23	130	75	19	7.780	0.0622	0.5009	1.3
Bottom	-	40	0.23	150	85	25	14.631	0.1889	0.5004	1.2

The models analyzed are shown in Figure 23. The length and height of the LMSG model Figure 23a are 346 and 200 m, respectively, with 17,696 elements. For the CLTCC model 23,076 elements are used as shown in Figure 23b. The LMSG panels superimpose at the end, while the CLTCC panels are isolated by a gate road pillar and the distance between the adjacent gate roads of the adjacent two panels is 10 m. A uniform stress of 20 MPa was applied to the top of the model corresponding to 800 m of overburden strata. Simulation was performed in five stages: (1) Loading the model to pre-mining state of stress without any excavation; (2) Only two development entries of the 1410 panel were excavated; (3) The 1410 panel was excavated; (4) Two development entries of the 1411 panel were excavated; and (5) The 1411 panel was excavated.

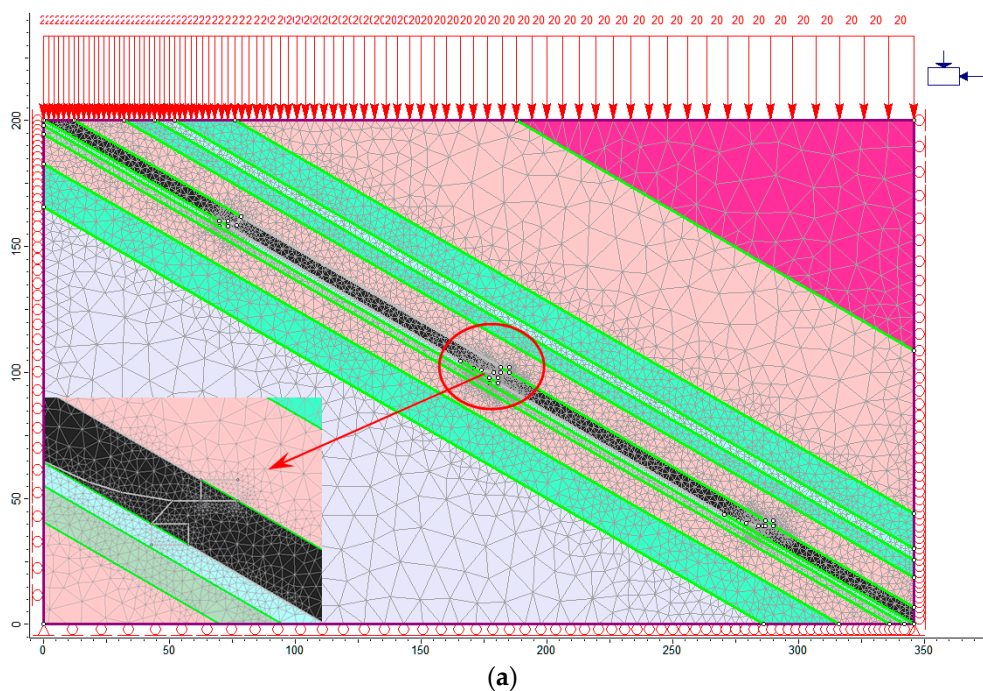


Figure 23. Cont.

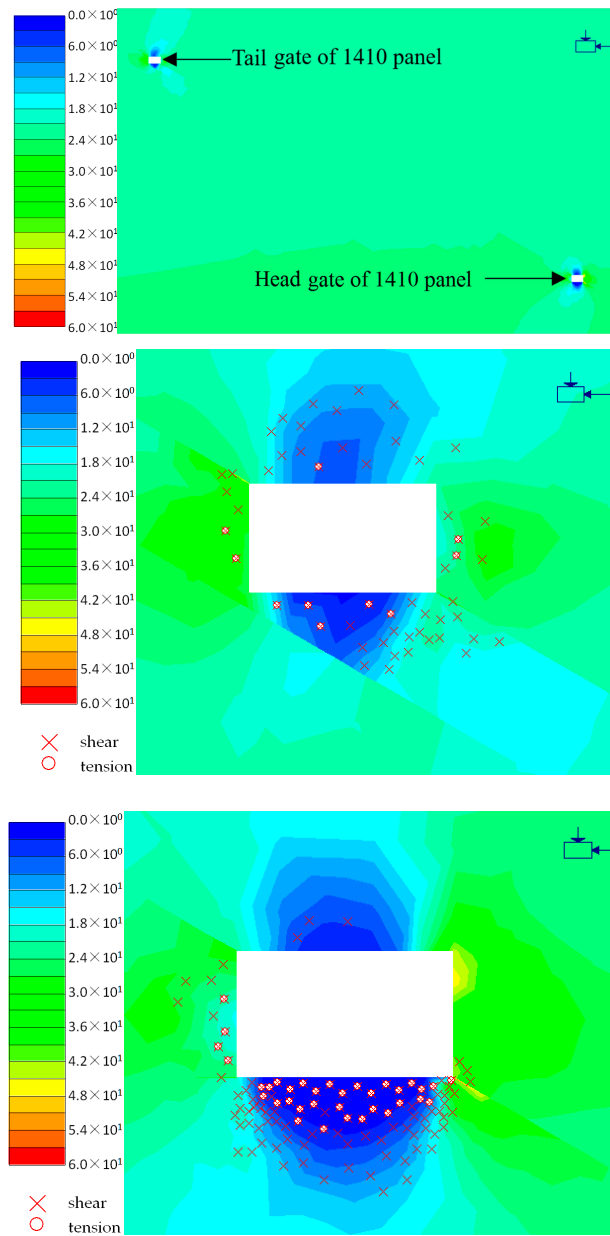
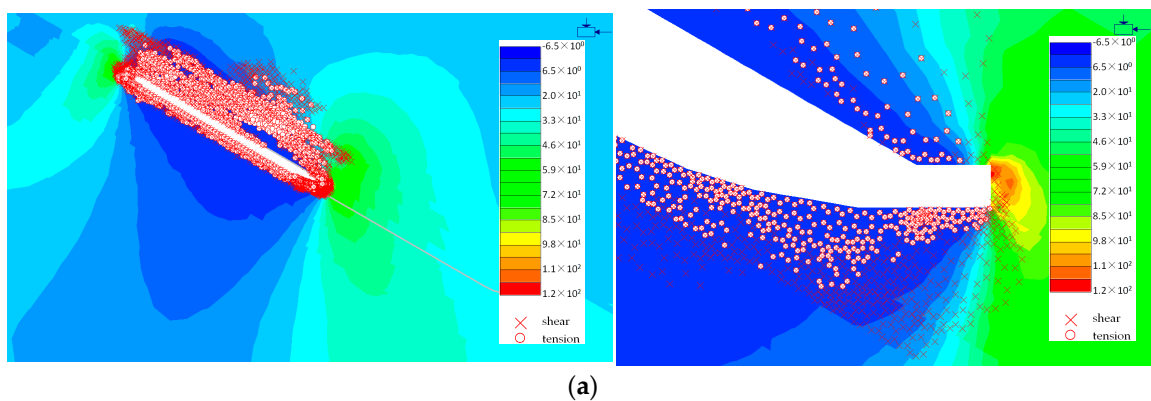


Figure 24. Vertical stress (MPa) and yielded elements around gate roads of the 1410 LMSG panel.



(a)

Figure 25. Cont.

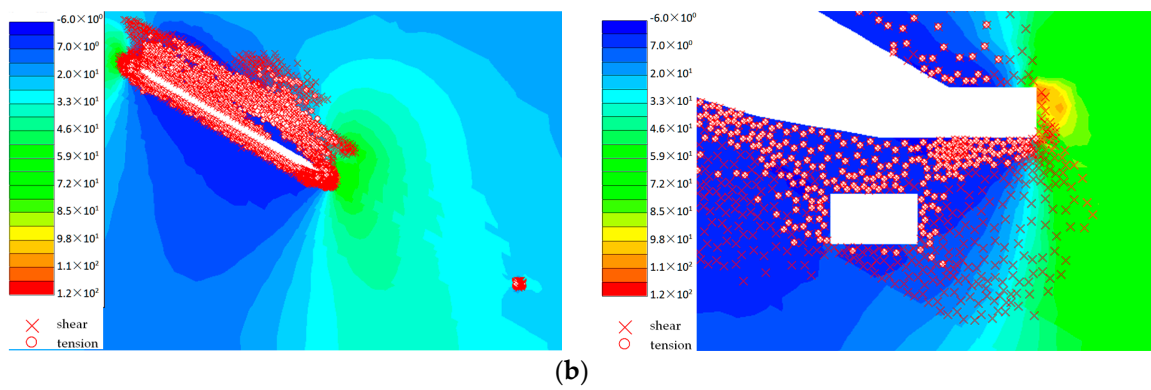


Figure 25. Vertical stress (MPa) and yielded elements after excavation of gate roads of LMSG 1411 panel. (a) Stress distribution and yielded elements after excavation of the 1410 LMSG panel; (b) stress distribution and yielded elements after excavation of gate roads of the LMSG 1411 panel.

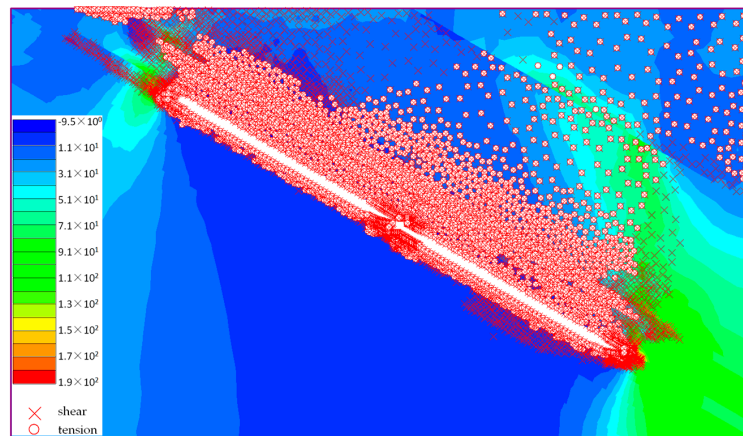


Figure 26. Stress distribution and yielded elements after two LMSG panels are mined out (MPa).

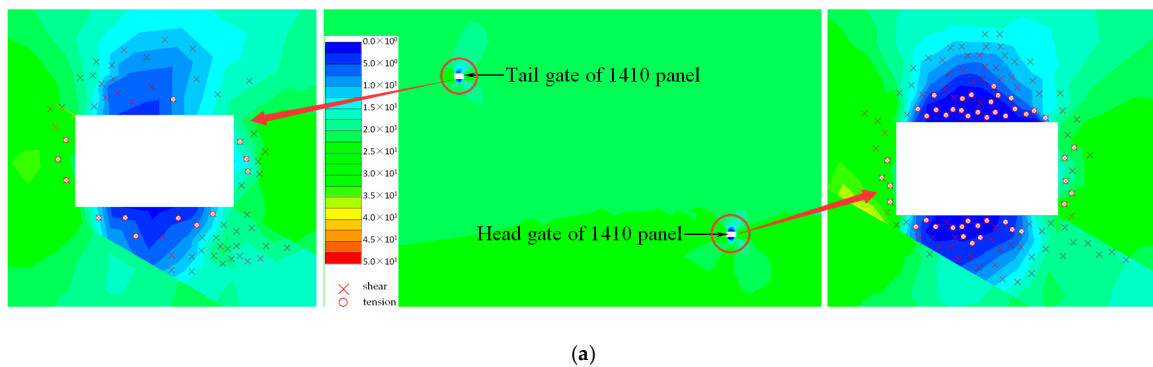


Figure 27. Cont.

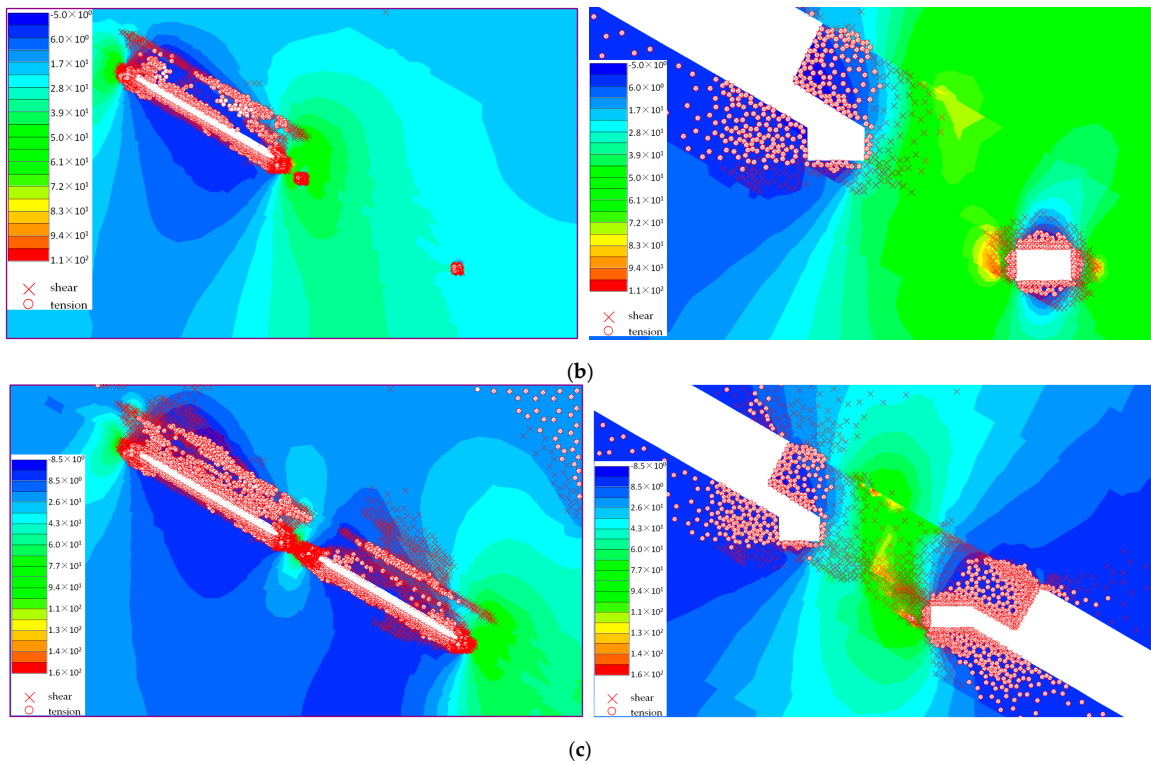


Figure 27. Excavation of CTLCC panels (MPa). (a) Stress distribution and yielded zones around gate roads of the 1410 CLTCC panel; (b) stress distribution and yielded zones after excavation of gate roads of CLTCC 1411 panel; (c) stress distribution and yielded zones after two CLTCC panels are mined out.

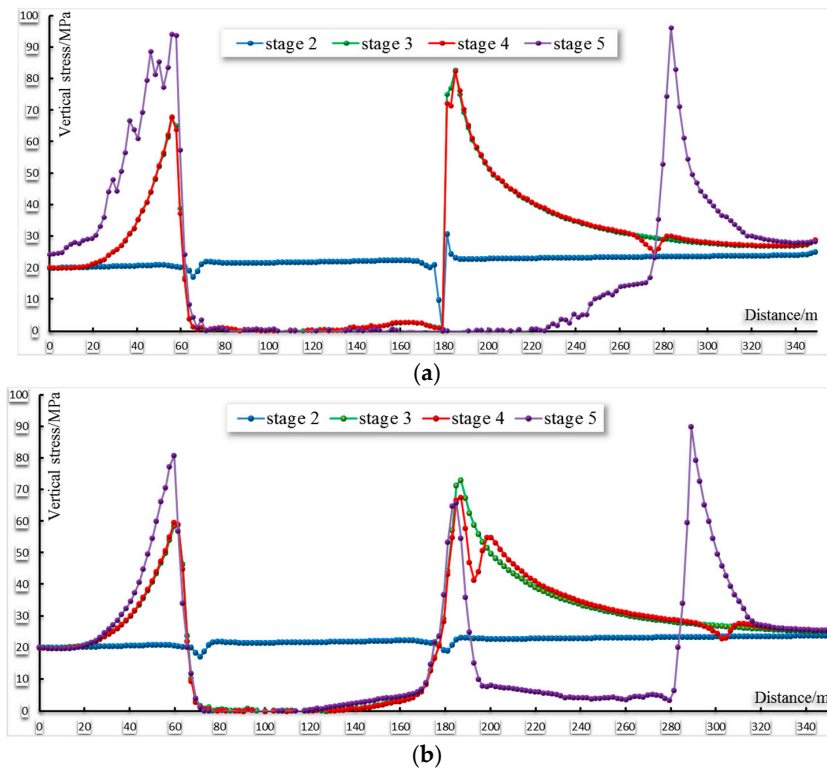


Figure 28. Vertical stress distribution in (a) LMSG; and (b) CLTCC.

Figure 25 shows that the tail gate of the 1411 LMSG panel is driven in a yielded zone. Thus some of the energy is dissipated before the tail gate of 1411 LMSG panel is excavated. Therefore, the tail gate of the 1411 LMSG panel is in a destressed zone. On the other hand, Figure 27 shows that the tail gate of the 1411 CLTCC panel is driven in a highly stressed elastic zone before the excavation of the tail gate of the 1411 CLTCC panel with a high likelihood of rock burst and sudden release of energy. This increases the likelihood of bursts for the tail gate. This is corroborated from field observations over the last decade where the excavation and maintenance of the tail gate for the CLTCC panels leads to rib sloughing and slabbing, large deformation, and coal bursts. However, no bursts occurred during the excavation and maintenance of the tail gate of the 1411 LMSG panel. The field tail gate profile is shown in Figure 29.



Figure 29. The field tail gate profile.

The LMSG alternate mining layout practiced in the case study mine was very successful based on the field observations. The proposed panel layout plays a critical role in improving stress environment for the gate roads in longwall mining. The 25110 fully mechanized panel in Yuejin coal mine (Figure 30) successfully adopted LMSG and experienced limited or no bursts in gate roads next to the gob. They pointed out that the LMSG not only reduces the cost, but also increases the coal recovery [11]. It has potential for widespread application in a variety of geological conditions. Many other coal mines have demonstrated the successful application of LMSG [14–23]. Figure 31 shows a 3D concept of LMSG, which should stimulate other discussion on alternate mining layouts [34]. Despite its many advantages, there are also some concerns and disadvantages about the LMSG technology. Coal mines currently using LMSG are all single-entry or two-entry layouts that may not be acceptable in some countries. Therefore, additional research should be done to assess the performance of three or four entry development entries to see if the approach is technically and economically feasible.

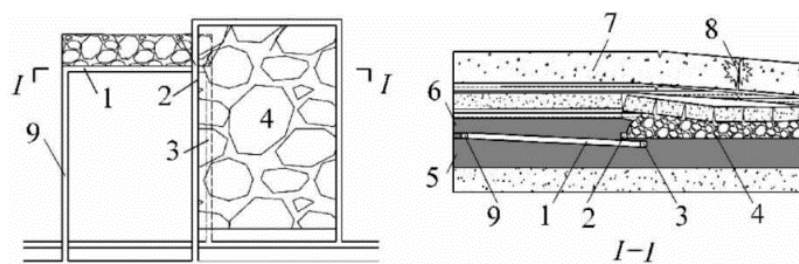


Figure 30. The application of LMSG in 25110 fully mechanized panel in Yuejin coal mine, China [11]. 1—Active face; 2—Head gate of the previous panel; 3—Tail gate of the successive panel; 4—Gob; 5—Bottom coal; 6—Top coal; 7—Sub key stratum; 8—Burst; 9—Head gate of the successive panel.

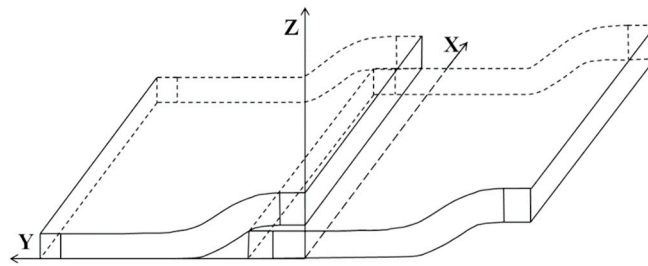


Figure 31. A block diagram of three-dimensional layout of LMSG.

9. Conclusions

This paper has presented a novel patented mining layout “Longwall Mining with Split-level Gate roads (LMSG)” for longwall development entries that has the potential to significantly improve ground control problems in mining of deep coal deposits subjected to high stress. LMSG locates gate roads on either end of a longwall panel at different vertical heights within a coal seam or in a geologically split seam, so that the two adjacent panels can be partially offset horizontally. By employing the multi slice longwall mining method locally at the face ends, adjacent panels overlap end to end, and pillar-less longwall mining is approached. The conventional rectangular gate road pillar is therefore transformed into a small triangular pillar, and the gate road of the subsequent panel is located along or under the gob of the previous mined-out panel where it is destressed.

The LMSG approach has sound scientific foundations as demonstrated through theoretical analysis, physical modeling and numerical modeling approaches, and demonstrated record of field applications. In Huafeng coal mine demonstrating LMSG the tail gates were located within the destressed zone with small roof support requirements minimal ground control problems. In addition, the stress concentrations within solid coal ahead of the active longwall face were smaller, wavy surface deformations were mitigated or eliminated, sliding of mining equipment downhill and disconnection of armored face conveyor (AFC) to the stage loader were significantly reduced along with increased recovery. The authors believe that the technology has potential to be utilized in other countries with similar geologic conditions.

Interested parties may contact Prof. Jingli Zhao regarding the intellectual property and application of technology in different settings.

Acknowledgments: This work was supported by the National Natural Science Foundation of China (Grant No. 51404270); Fundamental Research Funds for the Central Universities (Grant No. 2011YZ10) and China Scholarship Council (Grant No. 201506430011). The authors extend special thanks to Batugina Irina Mikhailovna, a member of Russian Academy of Natural Sciences who cooperated with one of the authors, Jingli Zhao, in doing research on dynamic disasters, prevention and control in Huafeng Mine.

Author Contributions: Jingli Zhao conceived the technology. All authors were involved in designing and carrying out the physical and numerical modeling studies. Pengfei Wang wrote the paper. Yoginder P. Chugh reviewed the technology concepts, outlined the paper, and performed significant review and editing of the technical paper.

Conflicts of Interest: The authors declare no conflict of interest.

References

1. Corkum, A.G.; Board, M.P. Numerical analysis of longwall mining layout for a Wyoming Trona mine. *Int. J. Rock Mech. Min. Sci.* **2016**, *89*, 94–108. [[CrossRef](#)]
2. He, M.C.; Xie, H.P.; Peng, S.P.; Jiang, Y.D. Study on rock mechanics in deep mining engineering. *Chin. J. Rock Mech. Eng.* **2005**, *24*, 2803–2813. (In Chinese).
3. Xie, H.P.; Zhou, H.W. Research and the thinking of deep coal mining and limit mining depth. *J. China Coal Soc.* **2012**, *37*, 535–542. (In Chinese).
4. Shabanimashcooln, M.; Li, C.C. Numerical modelling of longwall mining and stability analysis of the gates in a coal mine. *Int. J. Rock Mech. Min. Sci.* **2012**, *51*, 24–34. [[CrossRef](#)]

5. Schumachera, F.P.; Kim, E. Modeling the pipe umbrella roof support system in a Western US underground coal mine. *Int. J. Rock Mech. Min. Sci.* **2013**, *60*, 114–124. [[CrossRef](#)]
6. Qian, M.G.; Shi, P.W.; Xu, J.L. *Ground Pressure and Strata Control*; China University of Mining and Technology Press: Xuzhou, China, 2010. (In Chinese)
7. Suchowerskan, A.M.; Merifield, R.S.; Carter, J.P. Vertical stress changes in multi-seam mining under supercritical longwall panels. *Int. J. Rock Mech. Min. Sci.* **2012**, *61*, 306–320.
8. Chen, S.J.; Guo, W.J.; Cheng, G.Q.; Zhao, T. Research on Creep Supporting Effect of Deep Strip Pillar. *J. Min. Saf. Eng.* **2012**, *29*, 48–53. (In Chinese)
9. Dai, H.Y.; Wang, S.B.; Yi, S.H.; Kong, L.; Gao, Y. Influential laws on strata and ground movement of face-separated pillars at a great depth. *Chin. J. Rock Mech. Eng.* **2012**, *29*, 48–53. (In Chinese)
10. Peng, S.S. Topical areas of research needs in ground control—A state of the art review on coal mine ground control. *Int. J. Min. Sci. Technol.* **2015**, *25*, 1–6. [[CrossRef](#)]
11. Guo, X.P.; Dou, L.M.; Xu, B.G.; Tang, S.H.; Wen, X. Technology of Preventing Rock Burst by Lateral Layout Roadway near Goaf. *Coal Sci. Technol.* **2014**, *42*, 1–5. (In Chinese)
12. Yan, S.; Bai, J.B.; Wang, X.Y.; Huo, L. An innovative approach for gateroad layout in highly gassy longwall top coal caving. *Int. J. Rock Mech. Min. Sci.* **2013**, *59*, 33–41. [[CrossRef](#)]
13. Zhao, J.L. Whole Seam Longwall Mining with Split-Level Gate roads (LMSG) in Thick Coal Seams. China Patent ZL98100544.6, 18 February 1998. (In Chinese)
14. Wang, X.P. Discuss and practice of elaborate mining technology in Zhenchengdi mine. *Coal Sci. Technol.* **2011**, *39*, 9–11. (In Chinese)
15. Zhao, J.L.; Wang, P.F.; Su, Y. An innovative longwall mining technology in Tangshan coal mine, China. *Minerals* **2017**, *7*, 14. [[CrossRef](#)]
16. Niu, W.F. Prospect of roadway layout under conditions of thick coal seam with large dip angle. *Sci. Technol. Inf.* **2012**, *11*, 109–110. (In Chinese)
17. Zhao, J.L. Study on whole seam longwall mining with split-level gateroad. *J. China Coal Soc.* **2004**, *2*, 142–145. (In Chinese)
18. Zhang, J.C. Practice of LMSG in thick coal seams. *Inner Mong. Coal Econ.* **2014**, *12*, 108–161. (In Chinese)
19. Li, D.Z.; Gao, H.L.; Wang, H.W. Technology of Fall Prevention Antiskid to Equipment in Fully Mechanized Caving Coal Long Face with Large Angle. *Coal Sci. Technol.* **2013**, *41*, 75–77. (In Chinese)
20. Yang, J.W. Equipment Selection and Mining Technique of Fully Mechanized Top Coal Caving Mining in Steep Inclined Seam of Wangjiashan Mine. *Coal Sci. Technol.* **2011**, *4*, 48–50. (In Chinese)
21. Zhao, J.L. Development and Outlook of 3-D Stagger Arrangement Roadway Layout Technology. *Coal Eng.* **2014**, *46*, 1–3. (In Chinese)
22. Fan, X.M.; Zhao, J.L.; Wang, Y.B.; Wang, Z.Q. *Whole Seam Longwall Mining with Split-Level Gate roads and Its Application in Xishan Coal Mine Area*; China Coal Industry Publishing House: Beijing, China, 2013. (In Chinese)
23. Wang, P.F.; Hui, Q.B.; Zhao, K.C.; Wang, Z.Q. Optimization of gate road layout in mining of inclined coal seam at depth. *J. Liaoning Tech. Univ. Nat. Sci.* **2014**, *33*, 11–15. (In Chinese)
24. Zhao, J.L. Triple Sections Mining Technology (TSMT) in LMSG in Thick Coal Seams. China Patent 2004100395750, 10 February 2004. (In Chinese)
25. Ghabraie, B.; Ren, G.; Zhang, X.Y.; Smith, J. Physical modelling of subsidence from sequential extraction of partially overlapping longwall panels and study of substrata movement characteristics. *Int. J. Coal Geol.* **2015**, *140*, 71–83. [[CrossRef](#)]
26. Zhu, W.S.; Li, Y.; Li, S.C.; Wang, S.G.; Zhang, Q.B. Quasi-three-dimensional physical model tests on a cavern complex under high in-situ stresses. *Int. J. Rock Mech. Min. Sci.* **2011**, *48*, 199–209.
27. Shi, Y.W. *Ground Control Theory and Technology of Coal Mining Panel*; University of Mining and Technology Press: Xuzhou, China, 2003. (In Chinese)
28. Wang, Z.Q. *Study on Ground Pressure Behavior in LMSG in Thick Coal Seam*; China University of Mining and Technology: Beijing, China, 2009. (In Chinese)
29. Liu, H.W. *Mechanics of Material*; Higher Education Press: Beijing, China, 1999. (In Chinese)
30. RS². Available online: <https://www.rocscience.com/rocscience/products/rs2> (accessed on 10 October 2016).
31. Hoek, E.; Carranza, T.; Corkum, B. Hoek-Brown failure criterion—2002 edition. In Proceedings of the Fifth North American Rock Mechanics Symposium, Toronto, ON, Canada, 7–10 July 2002; pp. 267–273.

32. Hoek, E.; Diederichs, M.S. Empirical estimation of rock mass modulus. *Int. J. Rock Mech. Min. Sci.* **2006**, *43*, 203–215. [[CrossRef](#)]
33. RocData. Available online: <https://www.rocscience.com/rocscience/products/roccdata> (accessed on 10 October 2016).
34. Qiao, J. Julia Sets and Complex Singularities of Free Energies. *Am. Math. Soc.* **2015**, *234*, 1102. [[CrossRef](#)]



© 2017 by the authors. Licensee MDPI, Basel, Switzerland. This article is an open access article distributed under the terms and conditions of the Creative Commons Attribution (CC BY) license (<http://creativecommons.org/licenses/by/4.0/>).